*Available online at* www.scholarsresearchlibrary.com

Scholars Research Library

**Der Pharmacia Lettre, 2012, 4 (6):1888-1900**
***(http://scholarsresearchlibrary.com/archive.html)***

Scholars Research Library
ISSN 0975-5071
USA CODEN: DPLEB4

# Denovo *insilico* design of triazole analogs as reverse transcriptase inhibitors

**S Banerjee[1], S. Ganguly[2] and K. K. Sen[1]**

*[1]Department of Pharmacy, Gupta College of Technological Sciences, Ashram more, G.T. road, Asansol 713301, West Bengal, India.*
*[2]Department of Pharmaceutical Sciences, Birla Institute of Technology, Mesra, Ranchi 835215, Jharkhand, India*

---

**ABSTRACT**

*Non-nucleoside reverse transcriptase inhibitors (NNRTIs) have, in addition to the nucleoside reverse transcriptase inhibitors (NRTIs) and protease inhibitors (PIs), gained a definitive place in the treatment of HIV-1 infections. The present work deals with computational ligand docking methodology, AutoDock 4.0, based on Lamarckian genetic algorithm for virtual screens of a compound database of 36 entries (tri-substituted 1,2,4-triazoles) for novel and selective inhibitors of the enzyme Reverse transcriptase (PDB entry;1RT2), a potential anti-AIDs drug target. Considering free energy of binding and inhibition constant (KI) as a criterion of evaluation, a total of 34 compounds were predicted to be potential inhibitors of reverse transcriptase and 14 compounds displayed greater binding affinities than Nevirapine, a well-known reverse transcriptase inhibitor. Compound AM31, 2-{[4-amino-5-(2- hydroxyphenyl)-4H-1, 2, 4-triazol-3-yl]-thio}-N-(4-nitrophenyl)acetamide; compound AM33, 2-{[4-amino-5-(2-hydroxyphenyl)-4H-1,2,4-triazol-3-yl]-thio}-N-(4- methoxyphenyl) acetamide; and compound AM34, 2-{[4-amino-5-(2-hydroxyphenyl)- 4H-1,2,4-triazol-3-yl]thio}-N-(4-ethoxyphenyl)acetamide were considered to be the most potent reverse transcriptase inhibitors. Putative interactions between reverse transcriptase and inhibitors were identified by inspection of docking-predicted poses. Most of the compounds under study have shown significant binding energy as well as interaction in nanomolar range, thus suggesting the effectiveness of Autodock as an effective desktop molecular modelling tool. Attempts at discovering broad spectrum antiviral agents are presented herein.*

**Key words:** AutoDock 4.0; Reverse transcriptase; Lamarckian genetic algorithm; Nevirapine.

---

## INTRODUCTION

With the advent of high-performance and low-cost computing systems, exemplified by enterprise grid-based networks and large Linux farms, the past decade has been witness to a major change in the practice of molecular modeling in the pharmaceutical industry, particularly in the resources available to the computational chemist [1]. As a result, computational methods are being increasingly used in various stages of the drug-discovery process [2, 3]. Coupled with a rapidly rising number of protein structures, structure based drug design, driven by molecular docking and binding prediction has been undergoing somewhat of a renaissance. Molecular-docking methodologies ultimately seek to predict (or often retrospectively reproduce) the best mode by which a given compound will fit into a binding site of a macromolecular target. Docking, as a result, usually involves two independent steps: (1) the sampling of the ligand's positional, conformational, and configurational space to predict the ligand's pose within the

binding site of the receptor and (2) the scoring of the ligand's pose such that the ranking typically is an arbitrary reflection of how well a ligand is expected to bind to its cognate receptor. The re-emergence of such in-silico-based screening methods is of practical importance for lead-compound generation in drug discovery. Molecular-docking programs coupled with suitable scoring functions are now very much established as the necessary tools that enable computational chemists to rapidly screen large chemical databases and thereby identify promising candidate compounds for further experimental processing. A number of docking programs such as DOCK[4], FlexX[5], GOLD[6], AutoDock[7], GLIDE[8], QXP[9], and ICM[10] have been developed for just this purpose. Consequently, molecular docking has caught the attention of many pharmaceutical and biotechnology companies eager to discover novel chemical entities, and this has culminated in several well-documented comparative benchmarks on the relative performance of one docking code versus another, including various combinations of those noted above[11]. In the docking step, many ligand conformations are generated. There are several conformation sampling methods, such as genetic algorithms, Monte Carlo simulation, and simulated annealing. All sampling methods are guided by a function that evaluates the fitness between the protein and ligand. A rigorous search algorithm would exhaustively elucidate all possible binding modes between ligand and receptor. Autodock 4.0 uses GA as a global optimizer combined with energy minimization as a local search method[7]. It is almost 20 years since NNRTIs were identified as a new class of antiretroviral drugs for the treatment of HIV-1 infection[12]. Although they belong to different and diverse chemical families, they share a common and unique mechanism of action: their interaction with HIV-1 reverse transcriptase induces conformational changes that inhibit the catalytic activities of the enzyme. The Pol gene of HIV encodes three enzymes: the protease, the RT with embedded ribonuclease H (RNaseH) activity and the integrase. The HIV-1 RT is an asymmetric heterodimer, comprising a p66 subunit (560 amino acids) and a p51 subunit[13] (440 amino acids). Both subunits are encoded by the same sequence in the viral genome. RNAseH consists of the last (carboxy terminal) 120 amino acids of the p66 subunit, which correspond to the p15 fragment cleaved from the p66 subunit by the viral protease to generate the p51 subunit. Several crystal structures of free, unliganded HIV-1 RT have been solved[14-17]. The three-dimensional structure of the p66 subunit is often compared to a right hand (Fig. 1), with fingers (amino acids 1–85 and 118–155), a palm (amino acids 86–117 and 156–237) and a thumb (amino acids 238–318) domain[13]. The palm domain contains the polymerase active site with its three aspartic acids (110, 185 and 186) and the YMDD characteristic motif. Co-crystals of RT with a modified oligonucleotide and a dNTP[18] or double-stranded DNA[19] have revealed that the nucleic acid passes in the cleft behind the fingers and in front of the thumb domain. The catalytic pocket is formed by the fingers folding down into the palm domain, as observed in the RT-dNTP complex[18].

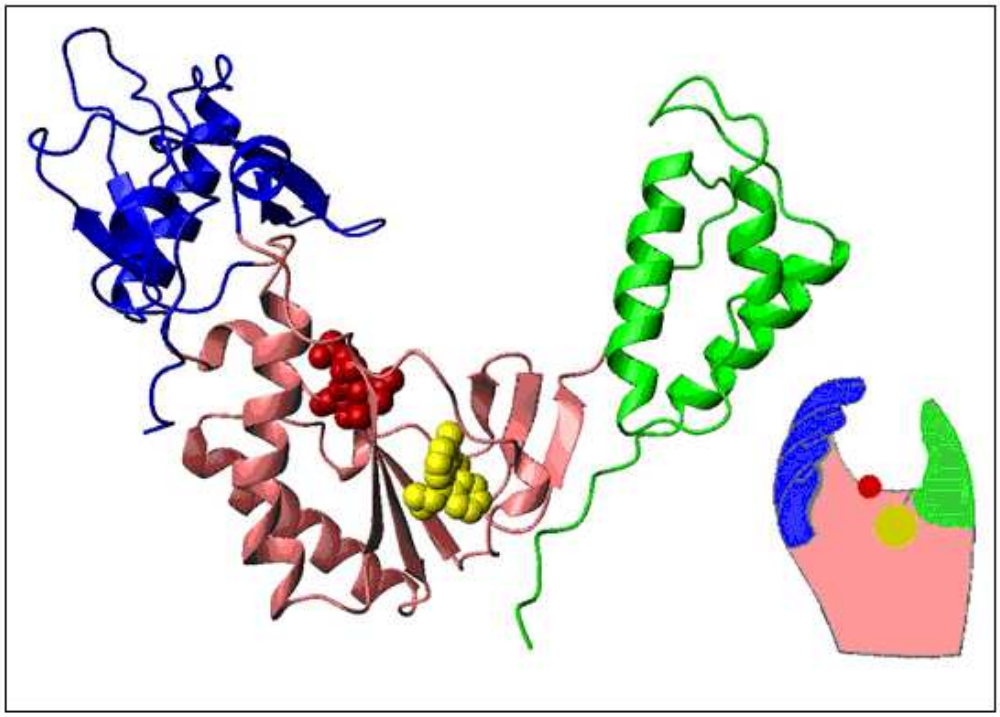

**Fig. 1: Ribbon representation of the active domain of Reverse Transcriptase[12]**

This ribbon representation of the RT active domain illustrates its hand-like structure, showing fingers (blue), palm (pink) and thumb (green). The active site (red atoms), where DNA is elongated, is in the palm region. Also shown is an RT-inhibitor drug (yellow) in the pocket where it binds. In this structure, the nucleic acid is located in front of both the fingers and the thumb. Next to the catalytic domain, the p66 subunit also contains the RNaseH domain (amino acids 427–560), linked to the former by the connection domain (amino acids 319–426). The connection domain is also involved in interactions with the nucleic acid and the p51 subunit. Despite their sequence homology, the p66 subunit assumes a flexible and open structure, whereas the p51 subunit is rather compact, and seems to play a structural role, devoid of catalytic activity, with the three aspartic acids buried inside[18]. Despite the chemical heterogeneity of NNRTIs, they all bind at the same site in the RT. This binding site is located in the palm domain of the p66 subunit of the heterodimeric protein, between the $\beta$6– $\beta$10– $\beta$9 and $\beta$12– $\beta$13– $\beta$ 14 sheets, and at the basis of the $\beta$4– $\beta$7– $\beta$8 sheet, at a distance of approximately 10Å from the catalytic site of the enzyme. This pocket is hydrophobic in nature and is lined by the aromatic (Y181, Y188, F227, W229, and Y232), hydrophobic (P59, L100, V106, V179, L234, and P236), and hydrophilic (K101, K103, S105, D132, and E224) amino acids of the p66 subunit, and two amino acids of the p51 subunit (I135 and E138). In the crystal structures of unliganded RT, the NNRTI binding pocket is not observed, but it is created when an inhibitor binds to the enzyme[13]. Indeed, the binding of an NNRTI induces a conformational change that rotates the side chains of the Y181 and Y188 amino acids up toward the catalytic site[15]. This results in a concomitant shift of the $\beta$4– $\beta$7– $\beta$8 sheet and the three catalytic aspartic acid residues of 2Å[14, 19]. These conformation changes, induced by the binding of the NNRTIs to the RT are thought to be at the basis of their inhibitory action against the enzyme. Noteworthy, the overall shape of the pocket does not vary significantly, even if the ligands are chemically very different.

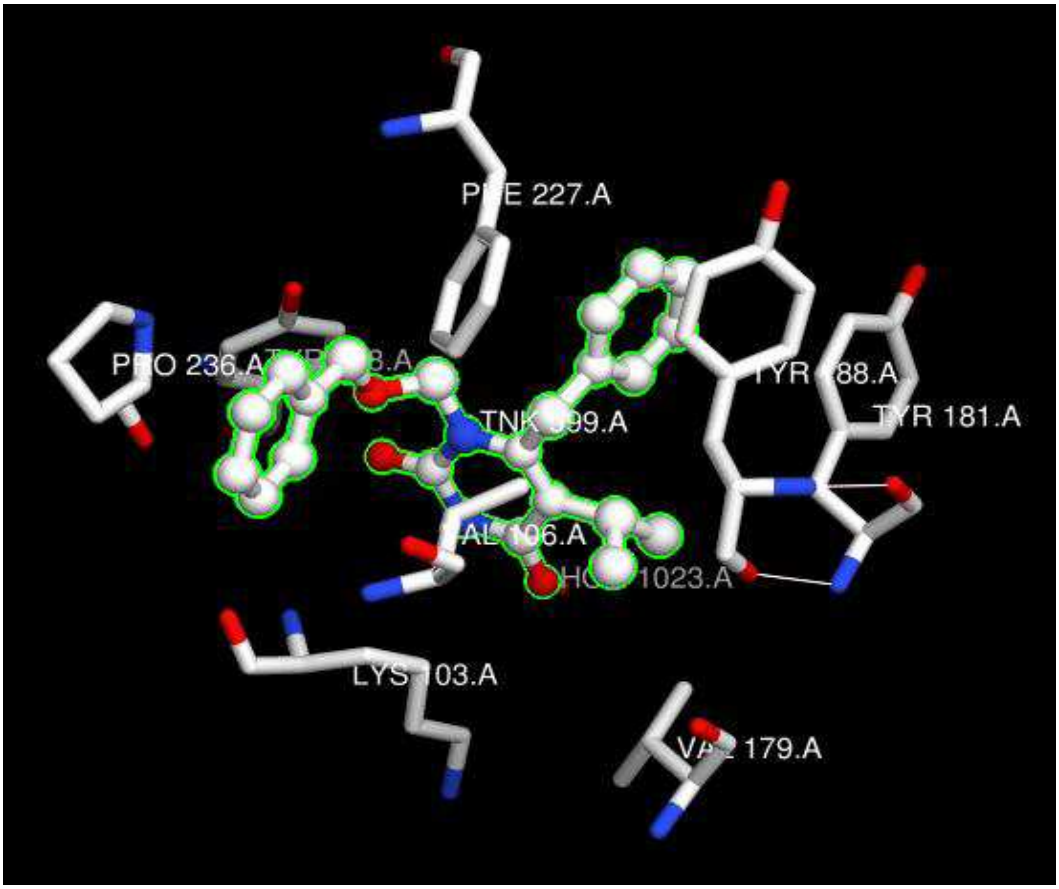


**Fig. 2: Key residues forming the NNRTI binding site from the 1RT2 X-ray structure for TNK–RT Complex (generated from chimera)**

To qualify as an NNRTI, the compound should interact specifically with (a non-substrate binding site of) the RT of HIV-1, and inhibit the replication of HIV-1, but not HIV-2 (or any other retrovirus) at a concentration that is significantly lower than the concentration required to affect normal cell viability[20]. Analysis of crystal structures

showed that first generation NNRTIs (TIBO, nevirapine, and α-APA compounds) bind to HIV-1 RT in a common ‘‘butterfly-like’’ conformation[21]. The relatively low potencies of these first generation NNRTIs against the common drug resistance mutations like Y181Cand Y188L/H, where favorable inhibitor–protein interactions were drastically reduced, sparked the search for new and more effective NNRTIs. The ITU (imidoythiourea) compounds, which were more flexible than their progenitors, were bound to HIV-1 RT in a unique ‘‘horseshoe’’ or ‘‘U’’ mode compared to the butterfly-like α-APA. In addition, the chemical stability of the imidoylthiourea moiety of the ITU derivative apparently was not optimal for an oral drug. Alterations of the imidoylthiourea complexes serendipitously led to the synthesis of a new diaryltriazine (DATA) class of compounds[22]. Replacement of the central triazine ring with a pyrimidine yielded a new class of diarylpyrimidine (DAPY) compounds that were more effective against both wild-type and drug-resistant HIV-1 strains when compared with corresponding DATA analogs. The concept of exploiting conformational degrees of freedom to offset the effects of resistance mutations may have broader implications for designing drugs against other rapidly evolving targets such as HIV protease[23] and targets from other infectious disease-causing agents. Although the enormous progress that has been made in the NNRTI field in recent years, especially in terms of the antiviral potency, the NNRTI clinical pipeline seems not to be that impressive as hoped. Most interestingly, few of the triazole derivatives have also been introduced in the discovery of reverse transcriptase inhibitors. A series of 3, 4, 5-trisubstituted 1, 2, 4-4H triazole derivatives[24, 25] was synthesized and investigated for HIV-1 reverse transcriptase inhibition.

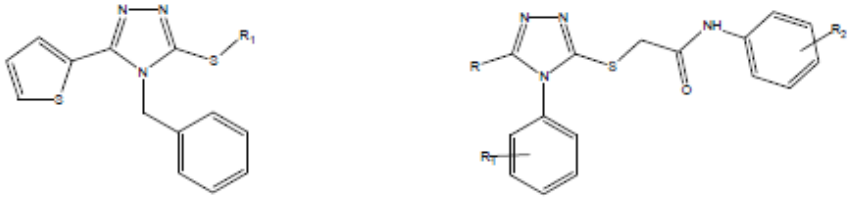

**Fig. 3: Chemical structures of triazole based reverse transcriptase inhibitors**

This improved activity profile against an nevirapine-resistant virus could prove extremely valuable, and warrants further studies on more nevirapine-resistant viruses. A number of improved compounds from this triazole scaffold are currently being considered for clinical evaluation. Considering the importance of triazole moiety in the field of developing robust reverse transcriptase inhibitors prompted us to built a pharmacophore, having a close resemblance with ‘‘butterfly-like’’ conformation, bearing triazole as a privilege scaffold as well.

## MATERIALS AND METHODS

### Reverse transcriptase enzyme modeling

The enzyme model was built by using AutoDock Tools- 1.5.1 and MGL Tools-1.5.4 packages (The Scripps Research Institute, Molecular Graphics Laboratory, 10550 North Torrey Pines Road, CA, 92037) running on Linux FEDORA 8.0. It consists of several steps. First, the 3D crystal structure of reverse transcriptase; PDB code 1RT2[26] was downloaded from Brookhaven protein data bank (PDB; http: //www.rcsb. org/pdb) and loaded to python molecular viewer. The nonbonded oxygen atoms of waters, present in the crystal structure were removed. After assigning the bond orders, missing hydrogen atoms were added, then the partial atomic charges was calculated using Gasteiger–Marsili method[27]. Kollman[28] united atom charges were assigned, non-polar hydrogens were merged, and rotatable bonds were assigned, considering all the amide bonds as non-rotatable. The receptor file was converted to pdbqt format, which is pdb plus ‘‘q’’ charges and ‘‘t’’ AutoDock type. (To confirm the AutoDock types, polar hydrogens should be present, whereas non-polar hydrogens and lone pair should be merged, each atom should be assigned Gasteiger partial charges). Since TNK, the co-crystallised ligand in the enzyme, 1RT2 (Fig. 2) is surrounded by few residues. Upon alignment of sequences in chimera, Lys 103 and Phe 227 have shown higher RMSD value; hence those two residues were included as flexible residue for introducing conformational search of flexible side chain. For the same macromolecule was saved in two files: one containing the formatted, flexible LYS 103 and Phe 227 residues and the other all the rest of the residues in the macromolecule.

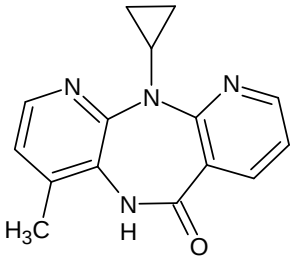


**Fig. 4: Chemical structure of Nevirapine**

**Validation of the docking protocol in Autodock**

The most suitable method of evaluating the accuracy of a docking procedure is to determine how closely the least energy conformation predicted by the scoring function resembles an experimental binding mode as determined by X-ray crystallography. In the present study, the docking of TNK 999 which was extracted previously from 1RT2 receptor complex into the RT was performed to test the reliability and reproducibility of the docking protocol for our study. We found a very good agreement between the localization of the inhibitor TNK 999 upon docking and from the crystal structure. The root mean square deviations (RMSD) between the predicted conformation and the observed X-ray crystallographic conformation of compound TNK 999 equaled 1.65 Å by Autodock. This indicated the reliability of the docking method in reproducing the experimentally observed binding mode for HIV-1 RT.

**Ligand receptor modeling**

CS ChemDraw 4.5 (Cambridge Soft.Com, 100 Cambridge park drive, Cambridge, MA 02140, USA) was used to draw 2D structures of different ligands. Ligands were further refined and cleaned in 3D by addition of explicit hydrogens by OpenBabel-2.2.1. All the structures were written in pdb file format. Autodock requires that ligands got partial atomic charges and Autodock atom types for each atom; it also requires a description of the rotatable bond in the ligand. Input molecules files for an Autodock experiments must confirm to the set of atom types supported by it. Autodock requires that ligands gave partial atomic charges and Autodock atom types for each atom; it also requires a description of the rotatable bond in the ligand. Autodock uses the idea of a tree in which the rigid core of the molecule is a ‘‘root,’’ and the flexible parts are ‘‘branches’’ that emanate from the root. This set consists of united atom aliphatic carbons, aromatic carbons in cycles, polar hydrogen, hydrogen-bonded nitrogen, and directly hydrogen-bonded oxygen among others, each with partial charges. Therefore, pdbqt format was used to write ligands, recognized by Autodock. Torsional degree of freedom (TORSDOF) is used in calculating the change in the free energy caused by the loss of torsional degree of freedom upon binding. In the Autodock 4.0 force field, the TORSDOF value for a ligand is the total number of rotatable bonds in the ligand. This number excludes bonds in rings, bonds to leaf atoms, amide bonds, and guanidinium bonds.

**Molecular docking studies**

AutoGrid 4.0[29] was introduced to pre-calculate grid maps of interaction energies of various atom types in all dockings, a grid map with 120*120*120 points, a grid spacing of 0.875 Å (roughly half of the length of a carbon–carbon single bond) were used, and the maps were centered on the macromolecule. In an AutoGrid procedure, the protein is embedded in a 3D grid and a probe atom is placed at each grid point. The energy of interaction of this single atom with the protein is assigned to the grid point. An affinity grid is calculated for each type of atoms in the substrate, typically carbon, oxygen, nitrogen, and hydrogens as well as grid of electrostatic potential using a point charge of +1 as the probe[30, 31]. Autodock 4.0[32, 33] uses these interaction maps to generate ensemble of low energy conformations.

It uses a scoring function based on AMBER force field, and estimates the free energy of binding of a ligand to its target. For each ligand atom types, the interaction energy between the ligand atom and the receptor is calculated for the entire binding site which is discretized through a grid. This has the advantage that interaction energies do not have to be calculated at each step of the docking process but only looked up in the respective grid maps. Since a grid map represents the interaction energy as a function of the coordinates, their visual inspection may reveal the potential unsaturated hydrogen acceptors or donors or unfavorable overlaps between the ligand and the receptor. Of the three different search algorithms offered by AutoDock 4.0, the Lamarckian Genetic algorithm (LGA) based on the optimization algorithm was used, since preliminary experiments using other two (Simulated annealing and genetic algorithm) showed that they are less efficient, utilizes (discredited) Lamarckian notation that an adaptations

of an individual to its environment can be inherited by its offspring. For all dockings, 100 independent runs with step sizes of 0.2 Å for translations and 5 Å for orientations and torsions, an initial population of random individuals with a population size of 150 individuals, a maximum number of 2.5*106 energy evaluations, maximum number of generations of 27,000, an elitism value of 1, and a number of active torsion of 5 were used. AutoDock Tools along with AutoDock 4.0 and Auto-Grid 4.0 was used to generate both grid and docking parameter files (i.e., gpf and.dpf files) respectively.

## RESULTS AND DISCUSSION

The results of LGA docking experiments of Reverse transcriptase inhibitors using AutoDock 4.0 and AutoGrid 4.0 are summarized in Table 1. For each docking experiment, the lowest energy docked conformer was selected from 100 runs. The central processing unit for a single docking experiment took 70-90 min, on a 2.19 GHz Intel (R) core2 Duo machine with 3.96 GB of RAM and Linux (FEDORA 2008) operating system.

**Table 1: Predicted Computational output of all compounds screened**

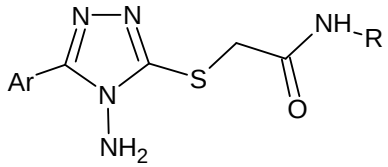


| Sl.no. | Compound | Ar | R | Observed binding energy(Kcal/mol) | Inhibition Constant(KI) | Docking Score |
|---|---|---|---|---|---|---|
| 1. | AM1 | Phenyl | o-bromoaniline | -9.46 | 115.74 nM | 20 |
| 2. | AM2 | Phenyl | p-bromoaniline | -10.03 | 44.20 nM | 09 |
| 3. | AM3 | Phenyl | o-nitroaniline | -9.78 | 68.32 nM | 11 |
| 4. | AM4 | Phenyl | p-nitroaniline | -9.45 | 118.23 nM | 21 |
| 5. | AM5 | Phenyl | o-anisidine | -9.29 | 153.83 nM | 25 |
| 6. | AM6 | Phenyl | p-anisidine | -8.81 | 347.00 nM | 28 |
| 7. | AM7 | Phenyl | p-phenitidine | -8.18 | 1.00 µM | 34 |
| 8. | AM8 | Phenyl | m-chloroaniline | -9.69 | 78.41 nM | 14 |
| 9. | AM9 | Phenyl | Benzylamine | -9.77 | 68.86 nM | 12 |
| 10. | AM10 | p-aminophenyl | o-bromoaniline | -9.70 | 77.87 nM | 13 |
| 11. | AM11 | p-aminophenyl | p-bromoaniline | -9.53 | 102.86 nM | 17 |
| 12. | AM12 | p-aminophenyl | o-nitroaniline | -8.77 | 375.31 nM | 29 |
| 13. | AM13 | p-aminophenyl | p-nitroaniline | -8.93 | 284.90 nM | 27 |
| 14. | AM14 | p-aminophenyl | o-anisidine | -8.45 | 636.46 nM | 33 |
| 15. | AM15 | p-aminophenyl | p-anisidine | -8.50 | 590.51 nM | 32 |
| 16. | AM16 | p-aminophenyl | p-phenitidine | -9.30 | 151.41 nM | 24 |
| 17. | AM17 | p-aminophenyl | m-chloroaniline | -10.03 | 16.16 nM | 08 |
| 18. | AM18 | p-aminophenyl | Benzylamine | -9.50 | 109.50 nM | 19 |
| 19. | AM19 | Pyridyl | o-bromoaniline | -9.53 | 102.78 nM | 16 |
| 20. | AM20 | Pyridyl | p-bromoaniline | -10.11 | 38.73 nM | 07 |
| 21. | AM21 | Pyridyl | o-nitroaniline | -9.31 | 149.34 nM | 23 |
| 22. | AM22 | Pyridyl | p-nitroaniline | -8.54 | 546.68 nM | 31 |
| 23. | AM23 | Pyridyl | o-anisidine | -9.11 | 211.52 nM | 26 |
| 24. | AM24 | Pyridyl | p-anisidine | -8.72 | 408.00 nM | 30 |
| 25. | AM25 | Pyridyl | p-phenitidine | -9.52 | 104.52 nM | 18 |
| 26. | AM26 | Pyridyl | m-chloroaniline | -9.96 | 50.36 nM | 10 |
| 27. | AM27 | Pyridyl | Benzylamine | -9.31 | 148.78 nM | 22 |
| 28. | AM28 | o-hydroxy-Phenyl | o-bromoaniline | -1.00 | 184.19 mM | 36 |
| 29. | AM29 | o-hydroxy-Phenyl | p-bromoaniline | -0.46 | 462.06 mM | 37 |
| 30. | AM30 | o-hydroxy-Phenyl | o-nitroaniline | -11.17 | 6.45 nM | 05 |
| 31. | AM31 | o-hydroxy-Phenyl | p-nitroaniline | -12.01 | 1.56 nM | 01 |
| 32. | AM32 | o-hydroxy-Phenyl | o-anisidine | -11.62 | 3.04 nM | 04 |
| 33. | AM33 | o-hydroxy-Phenyl | p-anisidine | -11.74 | 7.48 nM | 03 |
| 34. | AM34 | o-hydroxy-Phenyl | p-phenitidine | -11.94 | 1.76 nM | 02 |
| 35. | AM35 | o-hydroxy-Phenyl | m-chloroaniline | -1.14 | 146.94 mM | 35 |
| 36. | AM36 | o-hydroxy-Phenyl | Benzylamine | -10.58 | 17.44 nM | 06 |
| 37. | Nevirapine(reference) | | | -9.55 | 99.84 nM | 15 |

*a.*

*Potent Inhibitors*

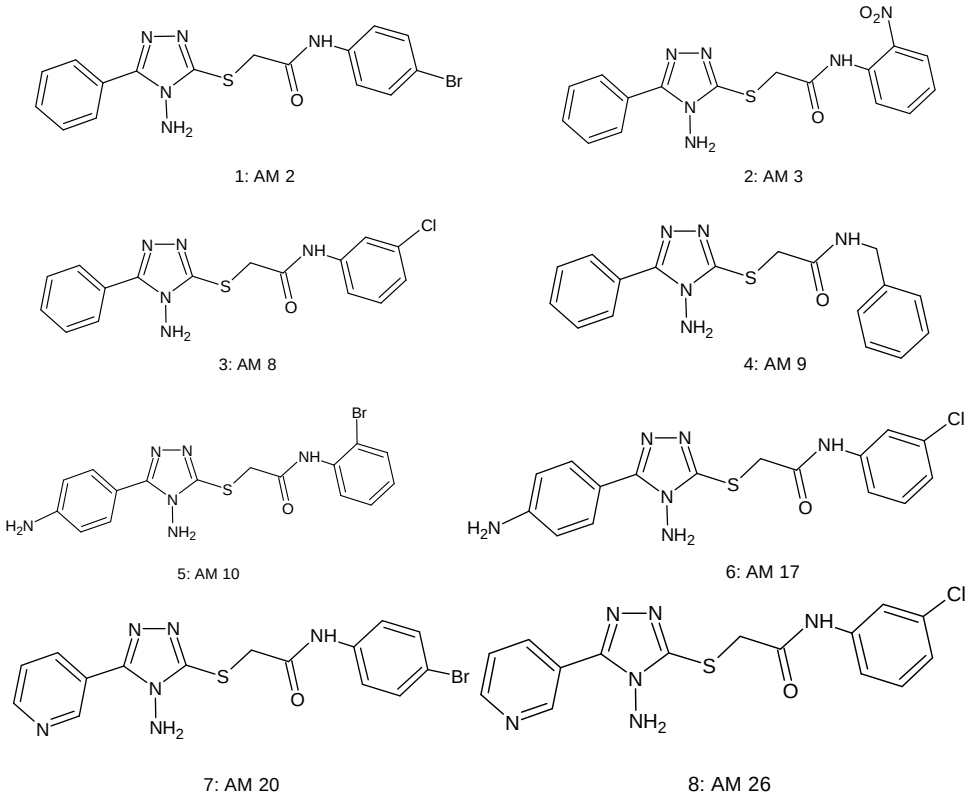


**Fig. 5 a, b, c, d: Chemical structure of triazole analogs with measurable potencies.**

Inhibitors 1–14 had KI values below 99.84 nM (‘‘potent inhibitors’’), whereas Inhibitors 15-36 had KI values more than 99.84 nM (‘‘weakinhibitors’’)

***b.***

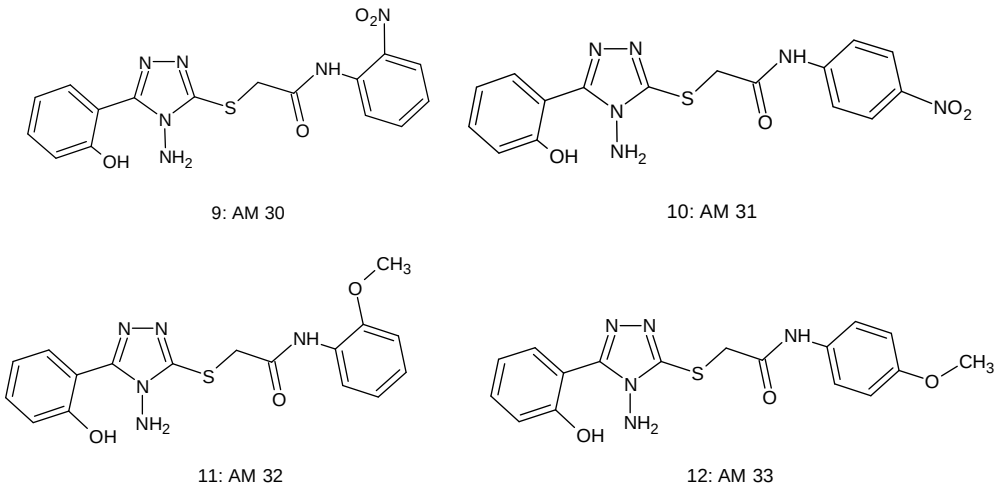

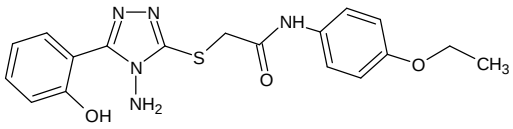

13: AM 34

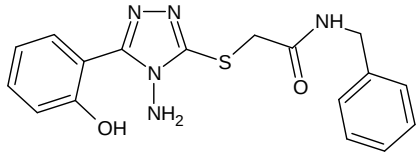

14: AM 36

*Weak inhibitors:*

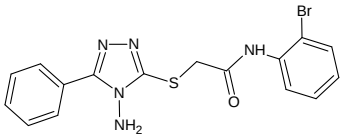

15: AM 1

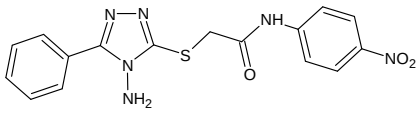

16: AM 4

**c.**

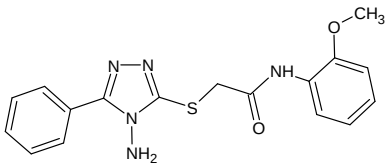

17: AM 5

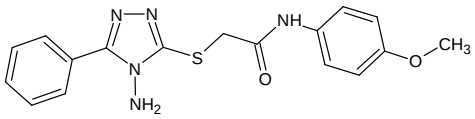

18: AM 6

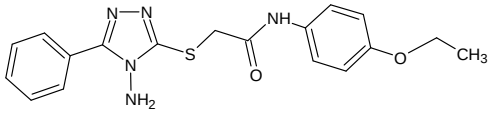

19: AM 7

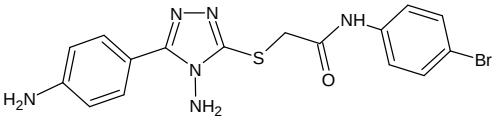

20: AM 11

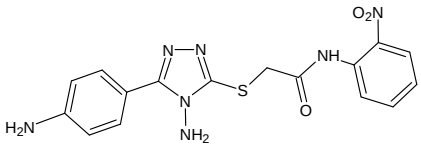

21: AM 12

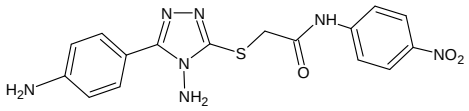

22: AM 13

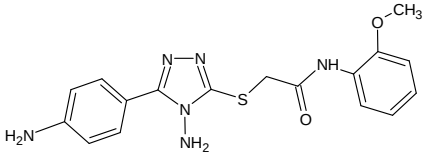

23: AM 14

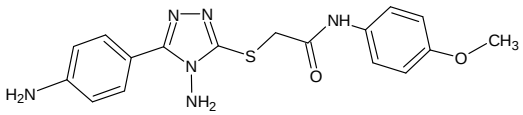

24: AM 15

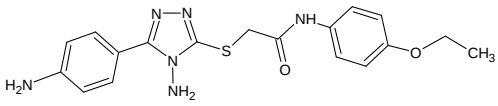

25: AM 16

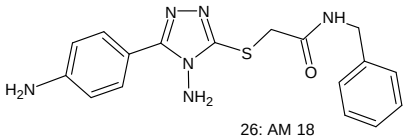

26: AM 18

d.

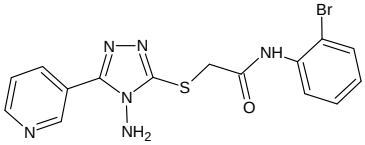

27: AM 19

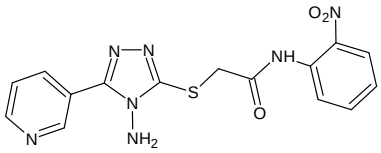

28: AM 21

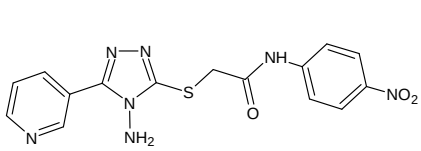

29: AM 22

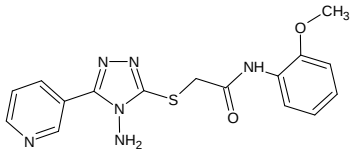

30: AM 23

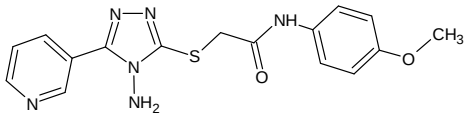

31: AM 24

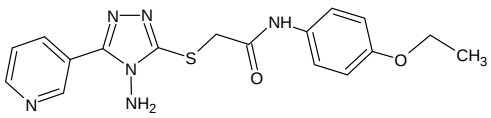

32: AM 25

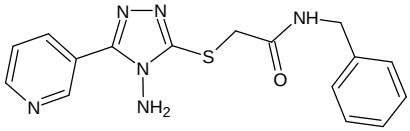

33: AM 27

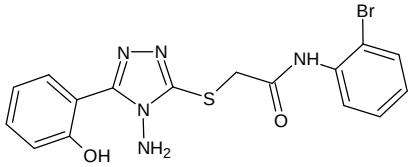

34: AM 28

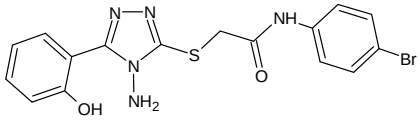

35: AM 29

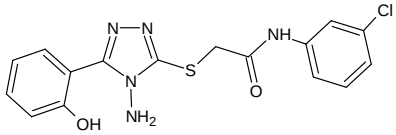

36: AM 35

In order to evaluate accuracy of docking, binding energy and numbers in cluster was used. Inhibition constant (KI) values were recorded for lowest binding energy mode. 14 molecules showed better inhibition potential than Nevirapine, a potent Reverse transcriptase inhibitor, with binding energy -9.55 kcal/mole. The chemical structures of all the 36 molecules are shown in the Fig. 5 Modeling and docking analysis revealed the nature of the active site and some key interactions that enabled the binding of triazole analogs to the active site.

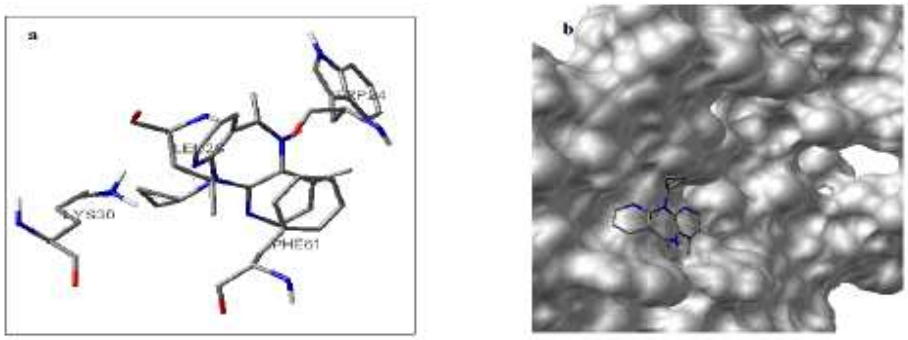


**Fig. 6: a(stereoview), b(molecular surface view) Docking predicted poses and interactions between Nevirapine and Reverse transcriptase**

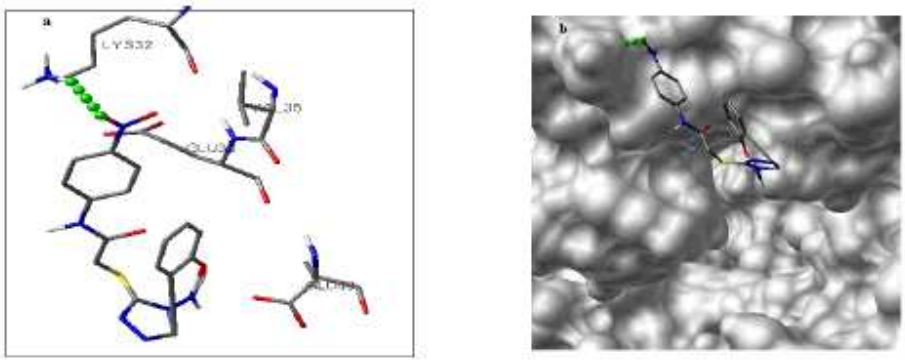

**Fig. 7: a(stereoview), b(molecular surface view) Docking predicted poses and interactions between AM31 and Reverse transcriptase**

All 37 molecules including the reference as Nevirapine were screened, the docking interactions of 2-{[4-amino-5-(2-hydroxyphenyl)-4H-1,2,4-triazol-3-yl] thio}-N-(4-nitrophenyl) acetamide (AM31),2-{[4-amino-5- (2-hydroxyphenyl)-4H-1,2,4-triazol-3-yl]thio}-N-(4-methoxyphenyl) acetamide (AM33), 2-{[4-amino-5-(2-hydroxyphenyl)-4H-1,2,4-triazol-3-yl]thio}-N-(4-ethoxyphenyl) acetamide (AM34) with lys 103 appeared to be in proximal vicinity and explains the higher selectivity to the enzyme. Docking poses and binding interactions of nevirapine AM31 and few other virtually potent inhibitors are shown in Figs 5, 6 and 7.

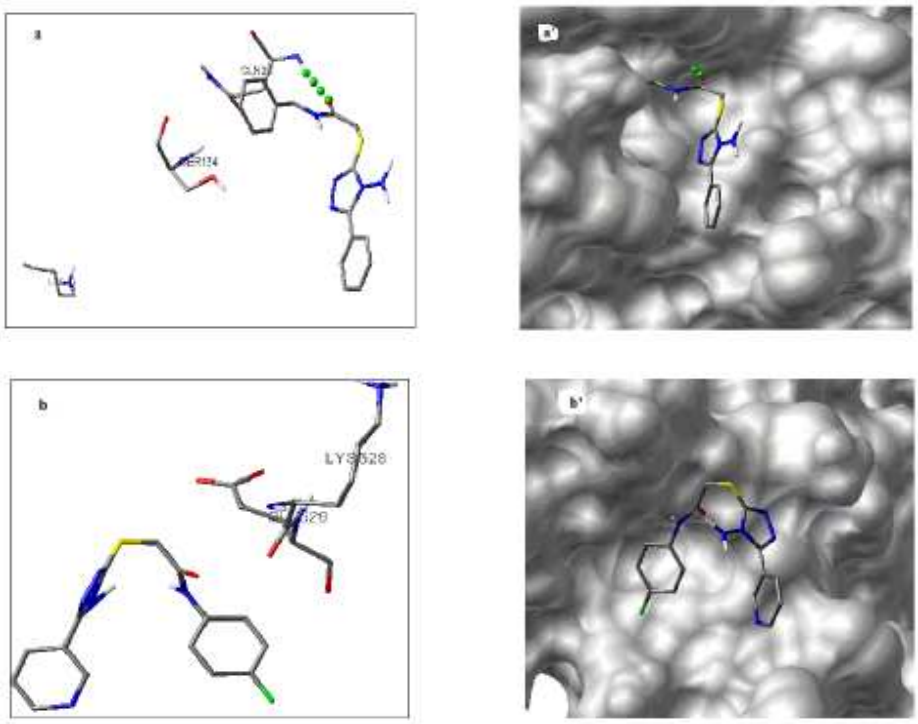

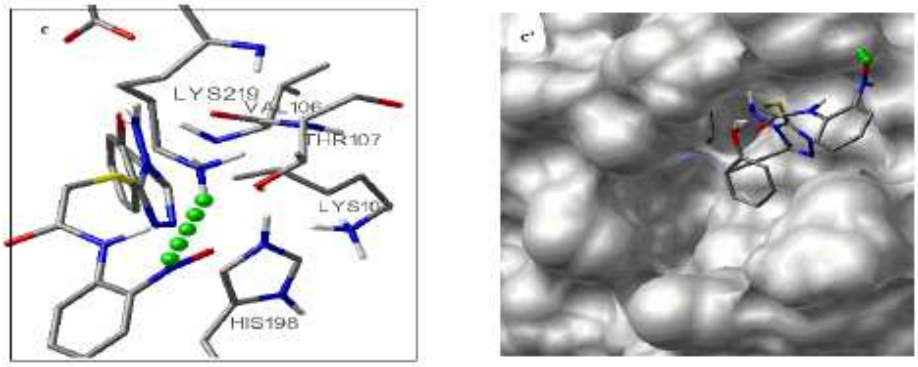


**Fig. 8 a-g: (stereoview), a'-g'(molecular surface view) Docking predicted poses and interactions between AM9,AM20, AM30, AM32, AM33, AM34 AM36, and Reverse transcriptase, respectively**

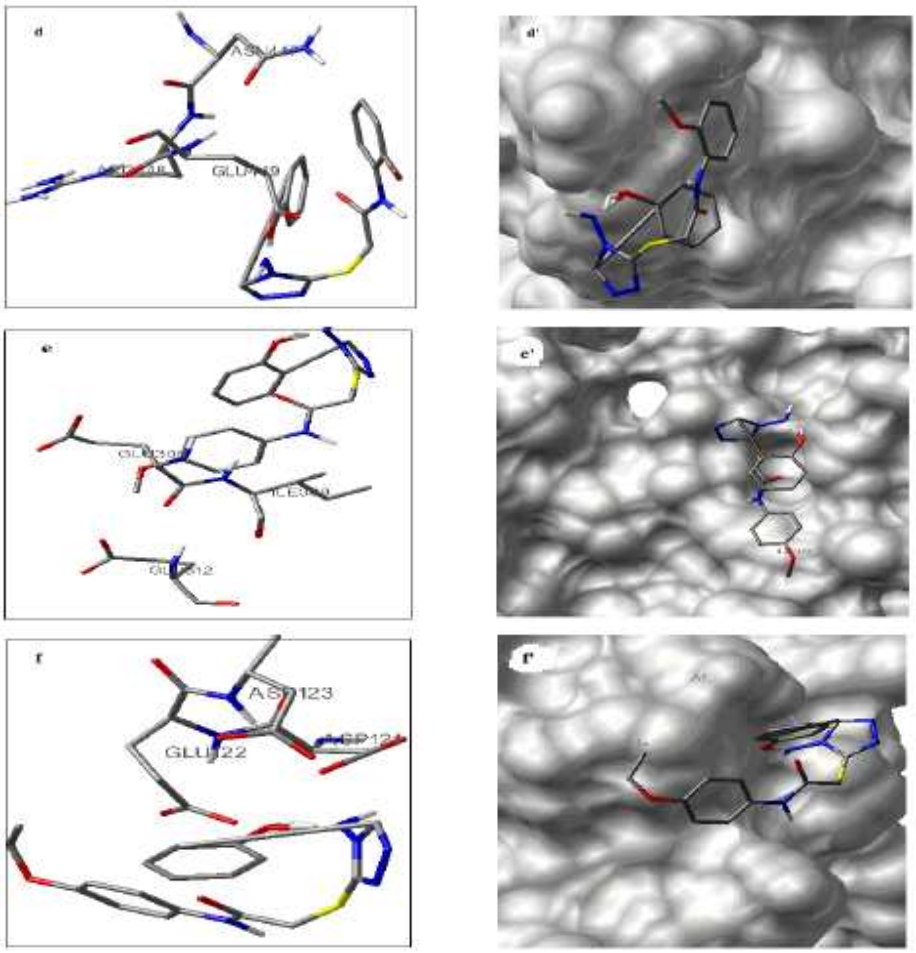

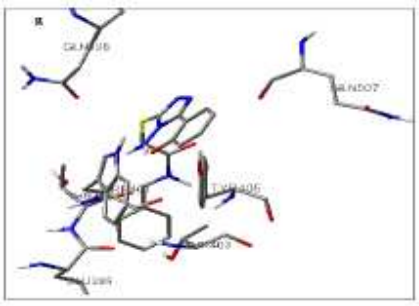

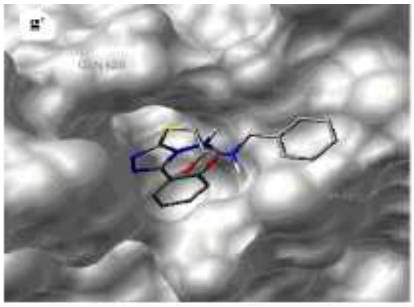

The compounds AM31, AM30, AM9 showed hydrogen bonding interactions with the residues LYS 32, LYS 219 and GLN23 respectively. The results summarized in Table 1, showed that 14 molecules among the 36 possesses better inhibition potential than the Nevirapine and majority of them were found in close proximity of Lys103 and Phe 227. This study contributes molecular insight into the binding process, which is of great importance for designing new ligands interfering with reverse transcriptase and shows that new wave of flexible ligand docking program like Auto- Dock can produce unbiased docking of Reverse transcriptase inhibitors in the enzyme active site. There is still significant space for improvement especially for the empirical binding free energy force field and KI prediction. The presence of various substitutents placed in both the aromatic ring was found to play a major role in determining inhibitory activity for Reverse transcriptase. The energy, KI values, and binding interactions revealed from docking poses provide the clues for the design of new molecules thus giving insight on structural requirement for designing more potent analogs. Although extensive efforts have been made in developing efficient molecules for the management of AIDS, search is still on as the virus undergoes rapid mutation making the existing drugs active only for a short span. These findings would be utilized for synthesizing and evaluating uncompromised novel reverse transcriptase inhibitors with all other possible modification.

**Acknowledgement**
The authors wish to thank Principal, Gupta College of Technological Sciences, Asansol. West Bengal, for providing necessary infrastructural and other facilities.

## REFERENCES

[1] R Abagyan, M Totrov, R Kuznetsov, *J Comput Chem*, **1994**, 15, 488-506.
[2] SA Allison, RJ Bacquet, JA McCammon, *Biopolymers*, **1998**, 27, 251–269.
[3] MP Bethune, *Antivir Res*, **2010**, 85, 75-90.
[4] E De Clercq, *Med Res Rev*, **1996a**, 16, 125–157.
[5] J Ding, K Das, H Moereels, L Koymans, K Andries, PA Janssen, SH Hughes, E Arnold, *Nat Structl Biol*, **1995a**, 2, 407–415.
[6] RM Esnouf, J Ren, C Ross, Y Jones, D Stammers, D Stuart, *Nat Structl Biol*, **1995**, 2, 303–308.
[7] RA Friesner, JL Banks, RB Murphy, TA Halgren, JJ Klicic;, DT Mainz, MP Repasky, EH Knoll, M Shelley, JK Perry, DE Shaw, P Francis, PS Shenkin, *J Med Chem*, **2004**, 47, 1739-1749.
[8] PJ Gane, PM Dean, *Curr Op in Strutcl Biol*, **2000**, 10, 401-404.
[9] J Gasteiger, M Marsili, *Tetrahedron*, **1980**, 36, 3219–3228.
[10] PJ Goodford, *J Med Chem*, **1985**, 28, 849–857.
[11] Y Hsiou, J Ding, K Das, AD Clark Jr, SH Hughes, E Arnold, *Structure*, **1996** 4, 853–860.
[12] H Huang, R Chopra, GL Verdine, SC Harrison, *Science*, **1998**, 282, 1669–1675.
[13] AL Hopkins, J Ren, RM Esnouf, BE Willcox, EY Jones, C Ross, T Miyasaka, RT Walker, H Tanaka, DK Stammers, DI Stuart DI, *J Med Chem*, **1996**, 39, 1589-1600.
[14] MA Jacobo, J Ding, RG Nanni, AD Clark Jr, X Lu, C Tantillo, RL Williams, G Kamer, AL Ferris, P Clark, *Proc Natl Acad Sci*, **1993**, 6320–6324.
[15] ID Kuntz, EC Meng, BK Shoichet, *Acc Chem Res*, **1994**, 27, 117-123.
[16] RT Kroemer, A Vulpetti, JJ McDonald, DC Rohrer, JY Trosset, F Giordanetto, S Cotesta, C McMartin, M Kihlen, PFW Stouten, *J Chem Inf Comput Sci*, **2004**, 44, 871-881.
[17] S Ganguly, N Panigrahi, *Int J Pharm tech Res*, **2009**, 1(4), 874-884.
[18] LA Kohlstaedt, J Wang, JM Friedman, PA Rice, TA Steitz, *Science*, **1992**, 256, 1783–1790.

[19] TA Kirschberg, M Balakrishnan, W Huang, R Hluhanich, N Kutty, AC Liclican, DJ McColl, NH Squires, EB Lansdon, *Bioorg & Med Chem Lett*, **2008**, 18, 1131-1134.
[20] DW Ludovici, RW Kavash, MJ Kukla, CY Ho, H Ye, BL De Corte, K Andries, M de Bethune, H Azijn, R Pauwels, HE Moereels, J Heeres, LM Koymans, MR de Jonge, KJ Van Aken, FF Daeyaert, K Das, E Arnold, PA Janssen, *Bioorg & Med Chem Lett*, **2001b**, 11, 2229–2234.
[21] S Makino, ID Kuntz, *J Comput Chem*, **1997**, 18, 1812-1825.
[22] GM Morris, DS Goodsell, R Halliday, R Huey, WE Hart, RK Belew, AJ Olson, *J Comput Chem*, **1998**, 19:1639-1662.
[23] C McMartin, RS Bohacek, *J Comp-Aided Mol Des*, **1997**, 11, 333-344.
[24] GM Morris, DS Goodsell, RS Halliday, R Huey, WE Hart, RK Belew, AJ Olson, *J Comput Chem*, **1998**, 19, 1639–1662.
[25] GM Morris, DS Goodsell, R Huey, AJ Olson, *j Comp Aided Mol Des*, **1996**, 10, 293–304.
[26] Ohtaka H, Xie D, E Freire, *Protein Science*, **2002**, 11, 1908–1916.
[27] M Rarey, B Kramer, T Lengauer, G Klebe, *J Mol Biol*, **1996**, 261, 470-489.
[28] DW Rodgers, SJ Gamblin, BA Harris, S Ray, JS Culp, B Hellmig, DJ Woolf, C Debouck, SC Harrison, *Proc Nat Acad Sci*, **1995**, 1222–1226.
[29] MDL Rosa, HW Kim, E Gunic, C Jenket, U Boyle, Y Koh, l Korboukh, M Allan, W Zhang, H Chen, W Xu, S Nilar, N Yao, R Hamatake, SA Lang, Z Hong, Z Zhang, JL Girardet, *Bioorg & Med Chem Lett*, **2006**, 16, 4444-4449.
[30] RK Scott, *Biosilico*, **2004**, 2, 175-179.
[31] K Sharp, R Fine, B Honig, *Science*, **1987**, 236, 460–1463.
[32] FJ Solis, RJ-B Wets, *Math Oper Res*, **1981**, 6, 19–30.
[33] SJ Weiner, PA Kollman, DA Case, UC Singh, C Ghio, G Alagona, S Profeta, PA Weiner, *J Am Chem Soc*, **1984**, 106, 765–784.